Applied Surface Science 680 (2025) 161310

Contents lists available at ScienceDirect

Applied Surface Science

journal homepage: www.elsevier.com/locate/apsusc

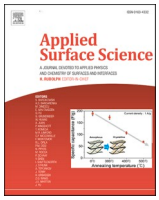

Full Length Article

Comprehensive study of SrF_2 growth on highly oriented pyrolytic graphite (HOPG): Temperature-dependent van der Waals epitaxy

Mauro Borghi [a], Giulia Giovanelli [b], Monica Montecchi [b], Raffaella Capelli [b], Andrea Mescola [c], Guido Paolicelli [c], Sergio D'Addato [c,d], Tibor Grasser [a], Luca Pasquali [b,e,f,*]

[a] Institute for Microelectronics (TU Wien), Gusshausstrasse 27–29, 1040 Vienna, Austria
[b] Department of Engineering "Enzo Ferrari", University of Modena and Reggio Emilia, Via Vivarelli 10, 41125 Modena, Italy
[c] CNR - Istituto Nanoscienze - Centro S3, Via Campi 213, Modena 41125, Italy
[d] Department of Physics, Informatics and Mathematics, University of Modena and Reggio Emilia, Via Campi 213/A, 41125 Modena, Italy
[e] Department of Physics, University of Johannesburg, P.O. Box 524, Auckland Park 2006, South Africa
[f] CNR - Istituto Officina dei Materiali (IOM), Strada Statale 14, Km. 163.5 in AREA Science Park, Basovizza, 34149 Trieste, Italy

A B S T R A C T

This study explores the molecular beam epitaxy (MBE) growth of SrF_2 on highly oriented pyrolytic graphite (HOPG) highlighting the temperature-dependent variations in growth morphology, crystalline structure and electronic properties. The comprehensive characterization of SrF_2/HOPG interfaces was carried out using atomic force microscopy (AFM), reflection high-energy electron diffraction (RHEED), ultraviolet photoelectron spectroscopy (UPS) and X-ray photoelectron spectroscopy (XPS). The spectroscopy data suggest that the chemical interaction of the fluoride with the substrate is weak at each deposited thickness and temperature of the substrate during the deposition, indicating a growth under a van der Waals epitaxial regime. SrF_2 nanostructures deposited on HOPG depict a distinctive bulk-like character, concerning their crystallinity and composition, even at the very initial growth stage. Remarkably, temperature plays a crucial role in driving the growth patterns, moving from coalescence of dendritic islands at room temperature to induce nearly 1D rows along the step-edges of HOPG terraces at higher temperatures (400 °C).

1. Introduction

Reducing the size of electronic devices preserving or improving their performance remains a technological challenge. With the ongoing miniaturization of devices, which are reaching dimensions of just few nanometres, Si/SiO_2 based devices are approaching their physical limits: charge mobility deteriorates [1] and the equivalent oxide thickness (EOT) has reached values of the order of one nanometre, which makes dielectric failures extremely easy. Silicon oxide is amorphous in devices, resulting in defective films. Moreover, the small permittivity becomes a problem when devices are scaled to few nm [2]. On the other hand, significant efforts are underway to introduce semiconducting materials other than silicon suitable for the nanoscale. In this respect, 2D semiconductors – e.g. transition metal dichalcogenides – are emerging as very promising candidates [3–6]. This would further require appropriate dielectrics to be coupled with these emerging classes of ultrathin semiconductors. A critical component of the basic electronic device, the field effect transistor (FET), remains the insulator, and those used in silicon technology poorly integrate with 2D semiconductors [7]. Among all the possible candidates that can address this issue, cubic ionic fluorides (like CaF_2 or SrF_2) may present several advantages [8–10] thanks to their high dielectric constant, the extremely wide band gap, and to the fact that ultrathin layers can be fabricated by molecular beam epitaxy (MBE), since they thermally evaporate in molecular form [11]. Additionally, thins films are crystalline and they are typically F-terminated at their outermost layer, with preferential growth direction along the [111] axis. In ideal conditions, when growth occurs along the [111] direction, there's no electric dipole perpendicular to the growth axis (considering sequences of F^--Ca^{2+}-F^- trilayers) and a self-passivation of the film is obtained. Consequently, the interaction of the fluoride film with the 2D semiconductors can be weak – van der Waals (VdW).

Besides this, to achieve high-performance devices and to move away from silicon technology, the integration of this type of dielectrics with conductive gate materials into a FET architecture is a mandatory step.

In this regard, we recently studied the growth modes of SrF_2 on Ag (111) by MBE as a function of the substrate temperature [12]. It has been observed that at room temperature (RT), the fluoride forms dendritic patterns, with many nanometric (111)-oriented islands which tend to merge and finally completely cover the substrate, as the nominal thickness of SrF_2 increases above few nm. When the substrate is heated

* Corresponding author at: Department of Engineering "Enzo Ferrari", University of Modena and Reggio Emilia, Via Vivarelli 10, 41125 Modena, Italy.
E-mail address: luca.pasquali@unimore.it (L. Pasquali).

https://doi.org/10.1016/j.apsusc.2024.161310
Received 24 July 2024; Received in revised form 11 September 2024; Accepted 21 September 2024
Available online 23 September 2024

during the deposition, the growth mode changes from a uniform film (at RT) to 3D islands, which evolve from pyramidal huts composed by SrF_2 (111)-oriented layers (at 250 °C) to triangular prisms which are rotated by 180° to each other at 400 °C [12].

In the present work, we extend our investigation choosing highly oriented pyrolytic graphite (HOPG) as the substrate. HOPG is a non-metallic conductive substrate that can be interesting for application and – to a certain extent – can emulate the growth modes that could occur on graphene. Many studies have already been reported regarding the deposition of insulating materials on HOPG, e.g., VO_x [13], SrO [14] and hBN [15] and on graphene [16,17]. Recently, the growth of CaF_2 on silicene was also studied [18], demonstrating that epitaxial growth is possible. The purpose of this work is, therefore, to investigate the formation of the SrF_2/HOPG interface as far as of the morphology and atomic geometry are concerned and consequently how this influences the electronic properties. Despite the large mismatch between the lattice parameters (2.46 Å for HOPG and 5.80 Å for SrF_2), graphite (graphene) is known to be weakly interactive with overlayers [19] and this peculiarity can lead to van der Waals (VdW) epitaxy and promote the formation of VdW heterostructures [17,20].

The same experimental methodology followed for the growth of SrF_2 on Ag(111) [12] has been adopted here. Specifically, SrF_2 was deposited in an ultra-high-vacuum (UHV) chamber by MBE on HOPG held at different temperatures, starting from RT and up to 400 °C. Electronic properties were investigated *in-situ* by x-ray and UV photoelectron spectroscopy, while structural and morphological properties were examined *in-situ* by reflection high energy electron diffraction (RHEED) and *ex-situ* by atomic force microscopy (AFM).

Different growth modes were observed. At 400 °C in particular, the flat HOPG terraces are almost free from the fluoride, which accumulates in the form of long parallel wires along the step edges of the terraces. This case can pave the way towards the growth of self-assembled 1D fluoride nanostructures, which represent a key challenge in the modern nanoscale industry.

2. Experiment

The technique used to deposit SrF_2 on HOPG is MBE, at a base pressure of $2 \cdot 10^{-10}$ mbar. The evaporations were carried out using a Knudsen cell equipped with a graphite crucible [21] loaded with fluoride crystals (MSE Supplies LLC, purity 99.99 %) that were heated to 1100 °C to allow sublimation.

The depositions were performed at different substrate temperatures, specifically RT, 200 °C and 400 °C and, for each temperature, different ultrathin thicknesses were investigated, between 0.5 nm and 5 nm. The evaporation rate was 0.2 nm/min, as evaluated with a quartz micro balance positioned close to the sample.

The HOPG substrate (Stanford Advanced Materials – ZYA grade) was prepared by mechanical exfoliation before each deposition, using an adhesive tape, and then annealed in UHV at 400 °C for 20 min. X-ray and ultraviolet photoelectron spectroscopy (XPS and UPS) were used to check the quality of the surface, investigating the valence band and the core levels of the substrate. The sample was heated thanks to a tungsten filament located adjacent to the HOPG backside and the temperature was measured with a K-type thermocouple in contact with the sample holder.

The electronic properties of the films were examined directly in situ immediately after growth by XPS and UPS. UPS spectra were obtained using He I photons ($h\nu = 21.2$ eV) generated by a windowless differentially pumped Vacuum Generator UV discharge lamp. The sample work function ϕ was evaluated by measuring the position of the secondary electron cutoff (E_{cutoff}), through linear extrapolation, relative to the Fermi energy (E_F), as measured on a clean gold reference: $\phi = h\nu - |E_F - E_{cutoff}|$. The secondary electron cut-off of the spectra was measured applying a bias of −10 V to the sample. XPS was performed with non-monochromatic Mg K_α photons ($h\nu = 1253.6$ eV) from a Vacuum Generators XR3 dual anode source ran at 15 kV, 17 mA. Data were collected with an Omicron EA125 electron analyser at normal emission. Resolution was varied from 50 meV in UPS to 0.5 eV in XPS.

After every deposition step, reflection high energy electron diffraction (RHEED) patterns were recorded in situ using a Perkin-Elmer model 06–190 electron gun, operated at 10 keV and at a grazing incidence angle of 2°. The RHEED screen was located 108 mm from the electron gun spot at the sample's centre.

The surface morphology was studied *ex-situ* using an Atomic Force Microscope (AFM) NT-MDT, NTEGRA AURA system. The AFM was operated in tapping (semi-contact) mode and measurements were performed in ambient conditions (T ≈ 25 °C, relative humidity ≈ 55 %) using rectangular shaped silicon cantilevers with nominal elastic constants between 0.3 and 0.8 N/m (MikroMasch HQ:CSC37/NoAl).

3. Results

3.1. Room temperature growth

In the following the growth mode of SrF_2 on HOPG is studied when the substrate is held at RT. First, the morphology and crystal structure of the film is addressed. Then, the electronic properties are studied through photoelectron spectroscopy.

3.1.1. Structural characterization

The left panel of Fig. 1 presents characteristic RHEED diffraction patterns captured at different SrF_2 growth stages. Fig. 1a displays the HOPG (0001) clean surface [13,14]. HOPG consists of (0001)-oriented crystallites with a low mosaic spread angle. In the basal plane the crystallites are oriented randomly. This implies that the pattern does not change with rotation of the crystal about its normal. In Fig. 1b, it can be noted that the diffraction pattern corresponding to SrF_2 (111) appears immediately after 0.5 nm of nominal coverage and it is superimposed to that of graphite, which is attenuated in intensity. When the film reaches the nominal thickness of 5 nm, the diffraction pattern shows that SrF_2 (111) and HOPG (0001) streaks are both still present and the diffraction pattern does not undergo drastic changes, as can be seen in Fig. 1c. The only difference compared to the 0.5 nm pattern is that the intensity of the fluoride-related streaks is predominant in comparison with that of graphite. The presence of highly modulated streaks, with quasi-transmission character and a broad specular beam, suggests that the surface is in a "mosaic island" configuration, i.e., a surface composed of fine (111)-oriented crystallites rotated by small angles around the axis perpendicular to the surface [22]. Also, the fact that HOPG (0001) features are still visible after the deposition of a film of 5 nm is a hint that the surface is not uniformly covered. Indeed, there are still uncoated substrate areas that contribute to the total RHEED pattern.

3.1.2. Surface morphology

To study the surface morphology of SrF_2 at different growth stages, AFM *ex-situ* was used. Fig. 1d displays the typical clean HOPG surface, taken after the mechanical exfoliation and after annealing at 400 °C. It reveals terraces ranging in width from 250 nm to 1 μm, separated by steps of about 0.3 nm in height, corresponding to the adjacent layer spacing in graphite.

Fig. 1e shows the initial growth of SrF_2, i.e., after the evaporation of 0.5 nm of nominal thickness. Unlike what was noticed on SrF_2 on silver [12], and on other fluoride-metal combinations [23–25], where the initial growth phase was represented by nanometric islands with an initially faint dendritic shape, on HOPG the fluoride islands grow right from the beginning with macroscopic dendrites where also the secondary dendrite arms are clearly visible. These structures with medium height of about 2 nm tend to develop almost perpendicular to the steps and they propagate from the step edges, which, in turn, are decorated by fluoride narrow wires. It is also possible to identify some nucleation centres in the middle of the terraces, far from the steps, as marked with

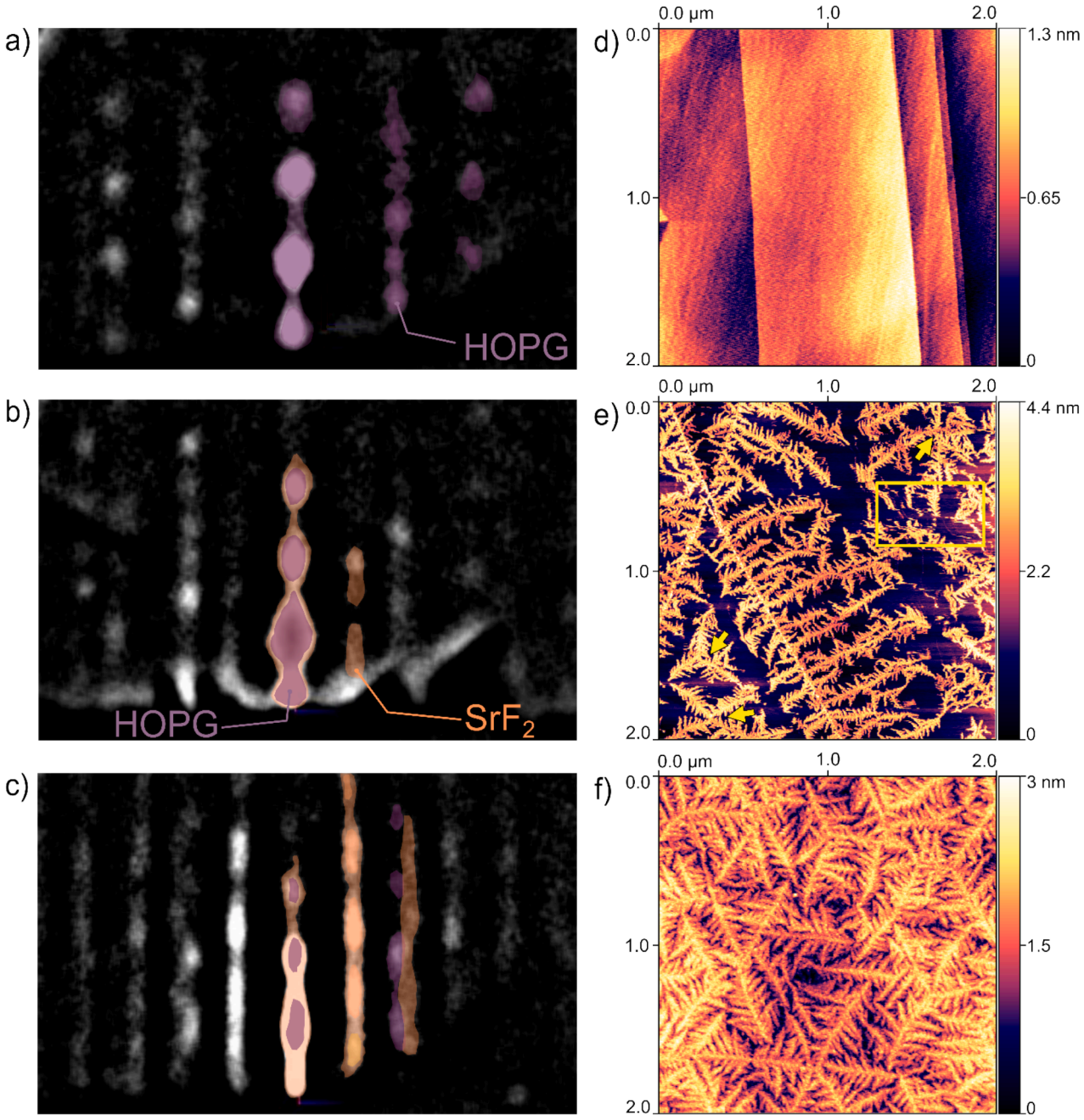

Fig. 1. a) RHEED diffraction pattern of HOPG after the annealing treatment; b) 0.5 nm nominal coverage of SrF_2 deposited at RT; c) 5.0 nm nominal coverage of SrF_2 deposited at RT. The HOPG diffraction pattern is highlighted in purple, while the SrF_2 characteristic streaks are highlighted in orange. AFM images of: d) clean HOPG; e) 0.5 nm of SrF_2 deposited at RT in morphology contrast. Yellow arrows indicate the nucleation centres inside the terraces, while the rectangle indicates the area where the fluoride is dragged by the AFM tip during the sweep; f) 5 nm of SrF_2 deposited at RT in morphology contrast. (For interpretation of the references to colour in this figure legend, the reader is referred to the web version of this article.)

yellow arrows, in which the dendrites propagate in the shape of stars with threefold to sixfold rotational symmetry. It is noteworthy that in some areas of the surface, e.g. in the region marked by the rectangle in Fig. 1e, during the AFM measurement the deposited fluoride was dragged by the tip. This fact denotes the weaker interaction of the fluoride with the substrate, as compared to metals like silver. This supports the idea of a weak VdW nature of the interaction between HOPG and SrF_2 [19].

Fig. 1f shows the morphology of the surface of the 5 nm film. The density of the dendritic islands has increased. The islands develop in 3D and tend to merge, almost covering the HOPG surface. Step edges of the substrate are no longer visible, and the star-shaped structures dominate. This leads to a rather defective film, in which the connections between the various converging dendrites leave large cavities. This is also the reason why, after the deposition of 5 nm of nominal thickness of SrF_2, HOPG diffraction streaks in RHEED are still visible, even if veiled, in Fig. 1c.

3.1.3. *Electronic properties*

Fig. 2a shows the UPS spectra of the pristine clean HOPG and after the deposition of different SrF_2 thicknesses. All the spectra have been normalized to the same secondary electron intensity peak. After the exfoliation and the degassing of HOPG, the UPS shows that the surface substrate is extremely clean, since its characteristics step structure at ~3

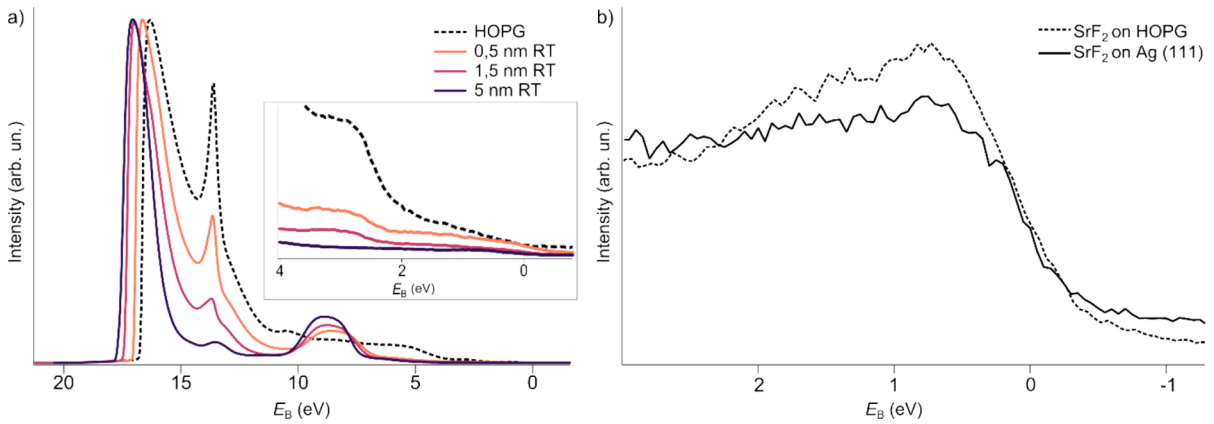

Fig. 2. a) UPS spectra showing the secondary electron cut-off of the pristine HOPG substrate and SrF_2 films at increasing thicknesses. The inset magnifies the region between 4 eV and 0 eV to evidence the characteristic HOPG structure at ~ 3 eV attributed to sp^2 hybridization and its attenuation after the deposition; b) Comparison of the low binding energy region just below the Fermi energy of SrF_2(5 nm)/HOPG (dotted line – present study) and SrF_2(5 nm)/Ag(111) (solid line – [12]).

eV attributed to sp^2 hybridization and the sharp peak at 13.7 eV associated with the σ* conduction band of HOPG are clearly visible [26,27]. This last feature has been interpreted in terms of inelastically scattered electrons populating conduction band states above the vacuum level [28]. Also, the measured HOPG work function has a value of 4.55 eV, which is consistent with that in the literature [26,27]. The intensity of the characteristic features of graphite decreases when SrF_2 is deposited on the surface and, at the same time, the F *2p* signal at about 8 eV emerges and increases with the film thickness. The low binding energy cutoff, as obtained by linear extrapolation on the low energy tail of the F *2p* band, indicates a valence band offset of 7.0 ± 0.1 eV, which agrees with recent predictions for fluorides on metals [29]. The fact that, even after the deposition of 5 nm of nominal thickness of fluoride, the carbon structure at 13.7 eV is still visible is compatible with the AFM and RHEED observations. The carbon signal comes from the gaps between the dendritic islands that, as they grow, do not uniformly cover the substrate. Interestingly, the high binding energy cutoff of the secondaries shifts progressively towards higher energies by 0.9 eV (with respect

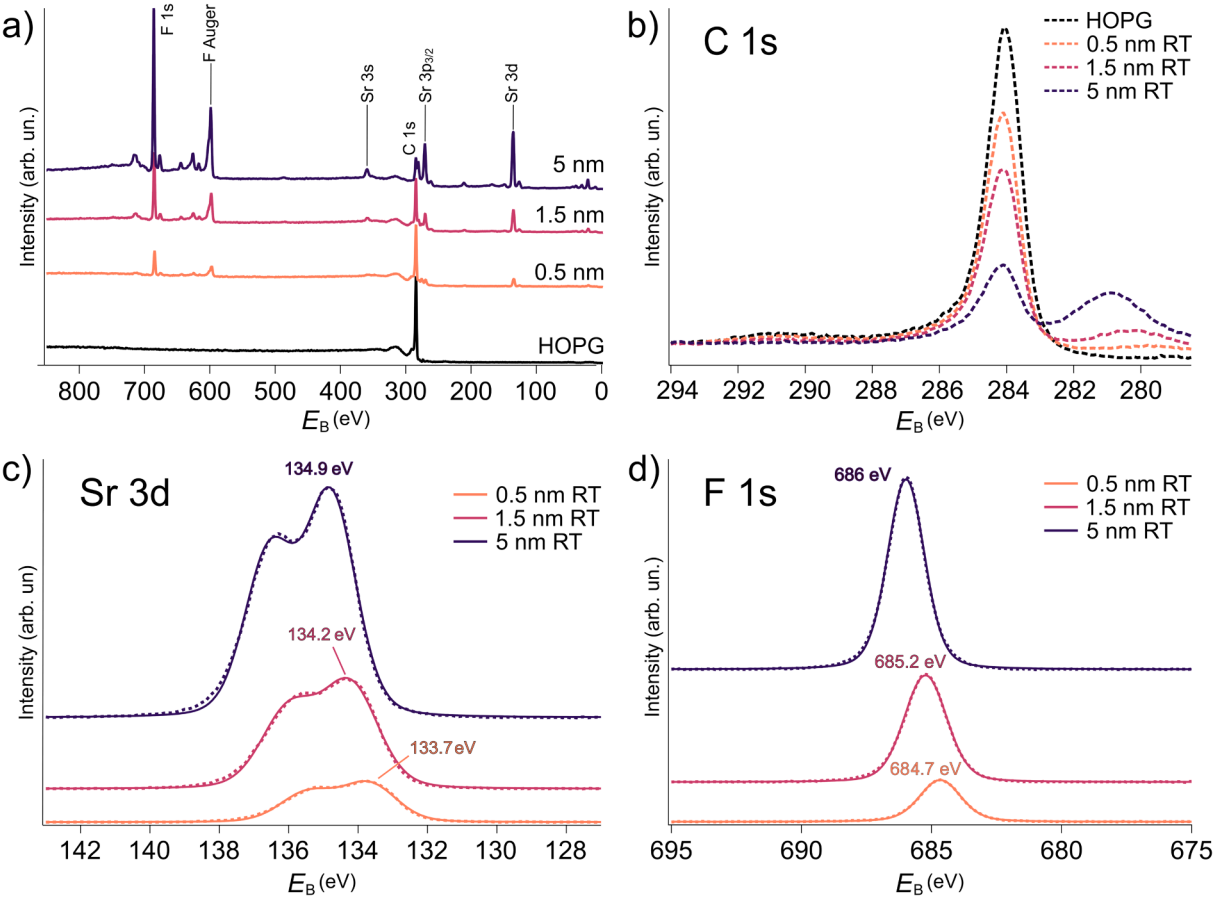

Fig. 3. a) XPS wide scans recorded as a function of nominal coverage; b) C 1*s* level of HOPG after removal of the Mg anode satellites; the structure emerging at increasing SrF_2 deposition at about 280–281 eV is associated to the contribution of Sr $3p_{1/2}$; c) Sr *3d* and d) F *1s* peaks, after removal of a Shirley-type background and the Mg anode satellite lines; the experimental data are represented by the dots, while the solid lines are the fitting.

to clean HOPG) with the increasing of nominal coverage. This in turn indicates a corresponding lowering of the vacuum level. This is associated with a 'push back' of the electronic charge of graphite due to the fluorine-terminated atomic layer of the fluoride at the buried interface, resulting in a reduction of the interface dipole even in the absence of a chemical reaction [30].

XPS measurements were also conducted after each evaporation step to examine the evolution of the core levels, as presented in Fig. 3. In Fig. 3a, the wide scan of HOPG shows the absence of contaminants before evaporation. Wide scans taken at different coverages further indicate a simultaneous attenuation of the carbon signal and an intensification of the Sr *3d* and F *1 s* peaks. No traces of oxygen or other contaminants are detected on the fluoride films.

Fig. 3b shows high resolution C *1s* spectra. The broad structure below 282 eV of binding energy is related to the emission from Sr $3p_{1/2}$, that increases progressively with coverage. C *1s* is centred at 284.2 eV, with the typical π-π satellite of graphite between 290 and 292 eV. Besides the reduction of the intensity, the energy position and the line shape of the C *1s* peak remain fixed to the HOPG values with varying film thickness, confirming the inertness of the carbon-fluoride interface.

The high-resolution Sr *3d* peaks are shown in Fig. 3c. The experimental data (dots) have been fitted with one Voigt doublet (solid line), which accounts for the spin–orbit splitting of 1.8 eV between the $3d_{5/2}$ and $3d_{3/2}$ states. This doublet is likely associated with Sr in the fluoride bulk, suggesting that SrF_2 tends to grow in a bulk-like configuration from the very initial growth phase. Similarly, the high-resolution F *1s* spectra, shown in Fig. 3d, have been fitted with a Voigt singlet (dots and solid lines), corresponding to the F bulk component in the fluoride.

The shift of 1.2 eV to higher binding energy observed both in the F *1s* ad Sr *3d* spectra can be ascribed, as already reported for the case of SrF_2 grown on silver, to defects emerging in the gap of the fluoride [12]. In ref. [12], the binding energy shift was attributed to the development of electronic states, eventually generated by defects, i.e. F vacancies, at boundaries between crystallites that merge and/or at the step edges of the terraces on top of the 3D fluoride islands that grow with their [111] axis perpendicular to the substrate plane. Regarding the effect of photon irradiation, we did not observe any evolution with time of the electron distribution curves, which seems to exclude radiation damage. The analogy with the case of silver is demonstrated in Fig. 2b, where the topmost part of the experimental valence band just below the Fermi energy is compared for films of 5 nm of nominal thickness grown on HOPG (dashed line – present work) and on Ag(111) (solid line – ref. [12]). The formation of a band of filled electronic states in the gap therefore induces a bending of the bands of the fluoride and generates the observed shift. On the other hand, AFM (Fig. 1e-f) clearly shows that the film is far from being uniform and flat, with the 3D islands developing already at very low coverage.

The stoichiometry of the overlayer in any case is always compatible with the SrF_2 bulk value, within the sensitivity of the technique, as evaluated from the intensity ratios of the Sr *3d* and F *1s* structures. This further indicates that the interface is inert with respect to chemical reactions and bonding.

3.2. High temperature growth

The same type of investigation carried out at room temperature was repeated with the substrate held at 200 °C and 400 °C.

3.2.1. Structural characterization and surface morphology

The substrate temperature during deposition plays a significant role in the growth mode of the films. Fig. 4a shows the RHEED pattern taken after the evaporation of 5 nm of SrF_2 with HOPG maintained at 200 °C. This pattern exhibits the characteristic streaks from both HOPG (0001) and SrF_2 (111), which are significantly modulated, like those observed at RT. The main difference between the patterns at RT and at 200 °C is that the HOPG features are clearly visible now, with their intensity not as attenuated by the fluoride film as for the RT case. This is consistent with AFM, Fig. 4c: at 5 nm of SrF_2 deposited at 200 °C the surface is

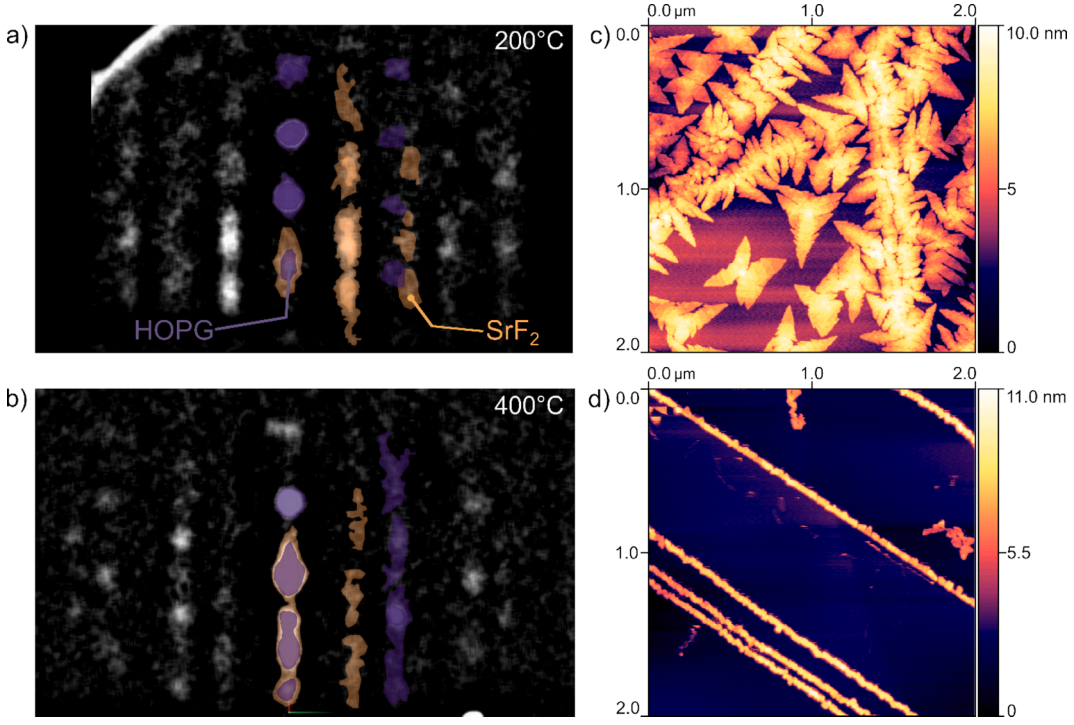

Fig. 4. a) RHEED diffraction pattern of 5 nm nominal coverage of SrF_2 deposited at 200 °C. The purple highlighted features indicate the HOPG diffraction spots while the orange ones identify the SrF_2 characteristic streaks; b) RHEED diffraction pattern of 5 nm nominal coverage of SrF_2 deposited at 400 °C; AFM topography images of c) 5 nm of SrF_2 deposited at 200 °C; d) 5 nm of SrF_2 deposited at 400 °C. (For interpretation of the references to colour in this figure legend, the reader is referred to the web version of this article.)

dominated by three-pointed star-shaped islands that are particularly dense at both sides of the HOPG step edges but also develop from nucleation centres within the terraces. The graphite signal remains clear because these structures, with heights between 4 nm and 5.5 nm, cover only approximately 58 % of the substrate surface. A detailed examination of these islands reveals that they consist of stepped huts, with step height of about 0.4 nm, originating from the adjacent (111) F-Sr-F trilayer planes of strontium fluoride, which grow along the [111] lattice direction.

The scenario changes significantly when evaporation is performed with the substrate temperature maintained at 400 °C. The SrF_2 streaks nearly disappear from the RHEED pattern (Fig. 4b), and the AFM image (Fig. 4d) shows that the HOPG surface is almost uncoated. The fluoride accumulates at the step edges of the substrate terraces, forming very long one-dimensional wires, ~ 6 nm high and 50 nm wide. In this case, apparently, the influence of temperature combined with the low reactivity of the graphite surface induces a very low sticking probability for the incoming molecules and promotes a high re-evaporation rate and a high mobility of the molecules, which only stick at the most active sites, i.e., the edges of the terraces, favouring the nucleation of the 1D fluoride wires.

3.2.2. *Electronic properties*

The high temperature depositions have also been investigated by UPS and XPS, which support the picture obtained by AFM and RHEED. Fig. 5a shows the evolution of the UPS at different coverages during deposition at 200 °C. The 13.7 eV feature of HOPG is still clearly visible even after depositing 5 nm of SrF_2. This happens because, consistent with the AFM of Fig. 4c, the surface of graphite is largely uncovered. In addition, this peak becomes predominant after growth of 5 nm at 400 °C (Fig. 5b). This, together with the low intensity of the F *2p* signal of the fluoride valence band, is consistent with the fact that the fluoride is basically confined in only small portions of the surface, i.e. in the form of wires at the graphite steps, as can be seen in Fig. 4d.

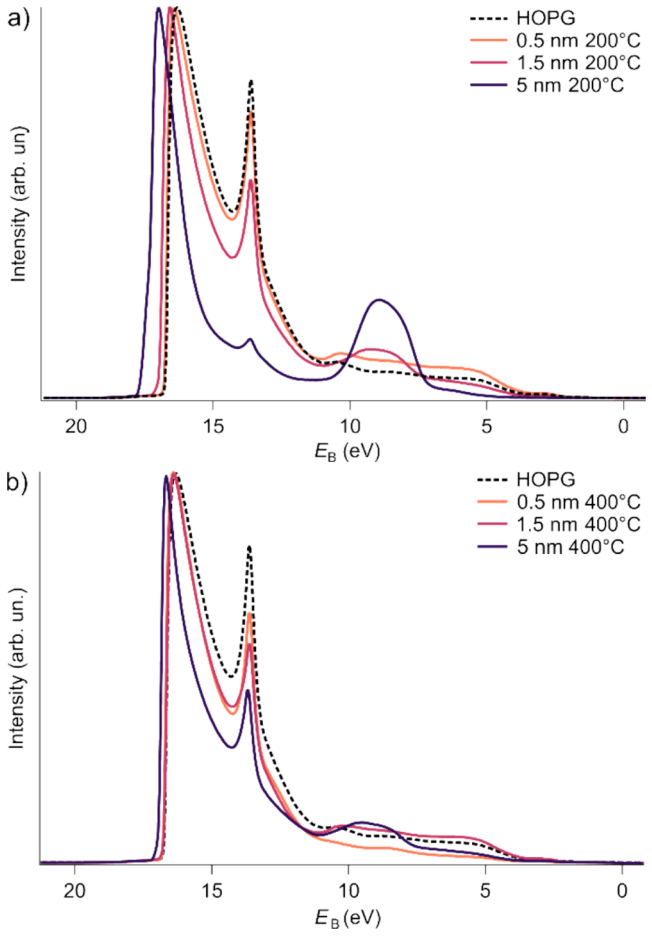

Fig. 5. UPS spectra taken at different coverages with the substrate temperature during the evaporation at: a) 200 °C and b) 400 °C.

Similarly to the RT case, the high binding energy onset of the UPS secondaries also shifts towards higer binding energy at increasing coverage during high temprature growth. However, compared to RT, the overall shift is reduced. At 200 °C, after 5 nm of coverage, this corresponds to 0.65 eV, and it reduces further to 0.15 eV at 400 °C. The evolution of the cutoff of the secondaries reflects the reduction of the work function averaged over the sampled area. This reduction is progressively less pronounced with the increase of the growth temperature because of the increasing presence of uncovered graphite regions.

The scenario that emerges from UPS is confirmed by XPS. The XPS wide spectra (Fig. 6a) and high-resolution peaks of C *1s* (Fig. 6b), Sr *3d* (Fig. 6c) and F *1s* (Fig. 6d) show that the temperature increase does not induce chemical reactions at the interface, at variance with respect to the SrF_2/Si system [21], and they confirm the weak interaction with graphite. More in detail, the wide spectra (Fig. 6a) clearly indicate that the overall amount of fluoride at the surface progressively reduces as the growth temperature is increased, despite the same nominal coverage of 5 nm. Consistently, the C *1s* peak gets more pronounced (Fig. 6b). The Sr *3d* spectra (dots in Fig. 6c) are fitted with only one Voigt doublet (solid line), that is related to the SrF_2 bulk. This also applies to the F *1s* peaks (dots in Fig. 6d), which has been fitted with one Voigt singlet (solid line). Interestingly, compared to the RT case, the energy position of the Sr $3d_{3/2}$ peak is slightly shifted towards lower binding energies, by 0.3 eV at 200 °C and by 0.4 eV at 400 °C. The same shift is observed for the F *1s* peak. This is interpreted in terms of a reduced bending of the bands during high temperature growth, i.e. a reduced number of filled electronic gap states associated to defects in the fluoride. This is due to the development of more definite and larger islands with respect to the RT case, as evidenced by AFM in Fig. 4, together with the large portions of the surface that remain uncovered.

Also, when the growth is carried out at high temperature the intensity ratios of the Sr and F peaks indicates that the fluoride stoichiometry is preserved at all coverages.

4. Discussion

Cubic ionic fluorides exhibit different bonding behaviour depending on the substrate. On semiconductors like silicon they may develop chemical bonds that favour almost ideal heteroepitaxial growth [31–33]. On metals like silver [12] or copper [24], weaker bonds induce the formation of sparse 3D islands which remain in any case coupled and aligned with the substrate in terms of the atomic geometry. On HOPG the interaction with the fluoride appears extremely weak (VdW). This induces a weak, or even negligible, geometrical coupling between the substrate and the overlayer. Already at RT the deposited fluoride molecules are highly mobile, compared to silver and copper. This is evidenced by the easiness of displacement of the fluoride by the AFM tip during scans (Fig. 1e), which was never observed for the case of SrF_2/Ag (111) at comparable experimental settings [12]. Due to the high mobility of the molecules, the fluoride islands nucleate at defect sites, mainly at the steps of the HOPG terraces. Compared to the growth over *3d* metals [1224], the density of the islands is lower at analogous nominal thickness, with the development of 3D crystallites at nucleation sites starting from the earliest deposition stages. The orientation of the fluoride islands seems independent on the substrate lattice, confirming the weak coupling with the substrate. The growth direction of the dendritic network is guided principally by the graphite steps, at least at low coverage. Even when the nominal coverage is increased, the islands do not cover the substrate uniformly, leaving a high density of voids. Moreover, when the substrate is heated during growth, the higher

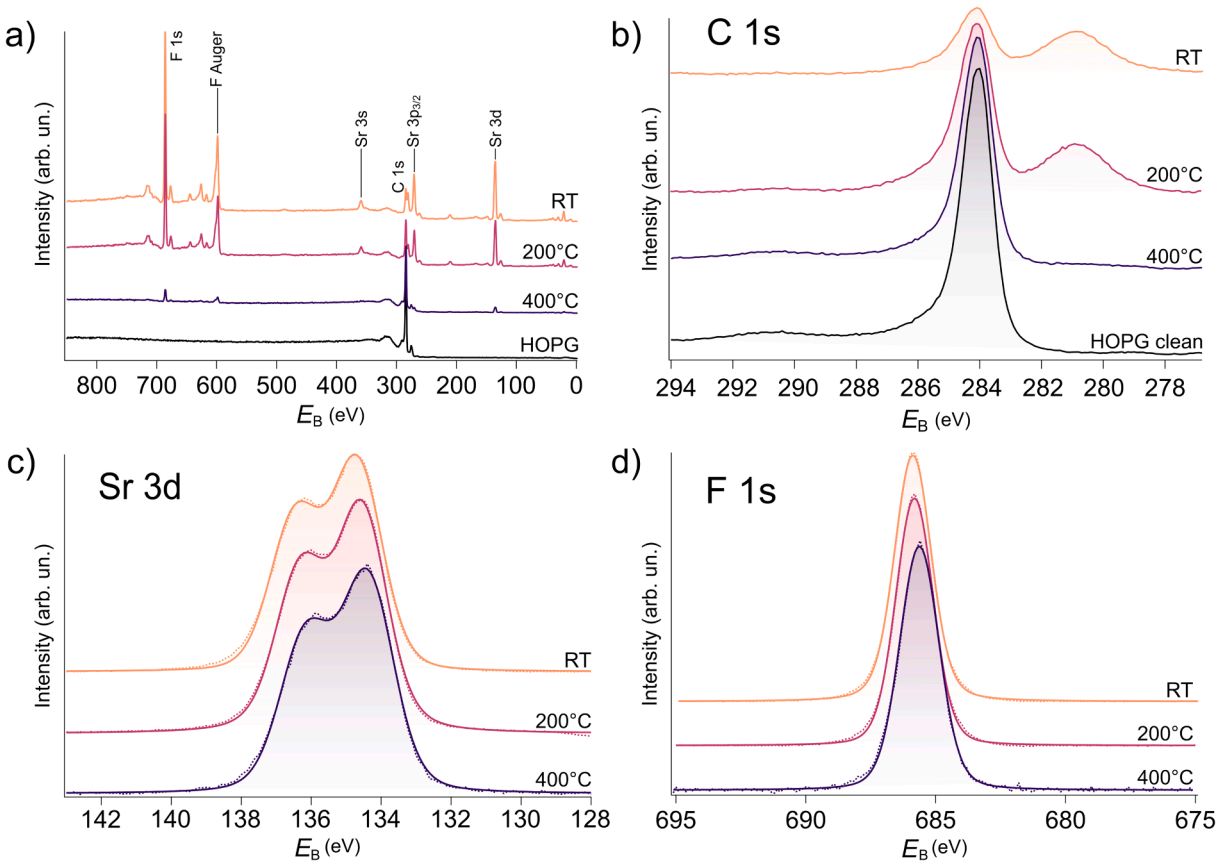

Fig. 6. a) Wide XPS spectra related to a nominal coverage of 5 nm grown at different substrate temperatures; higher resolution regions in correspondence of C 1*s*, Sr *3d* and F *1s* core levels are shown in panels b), c) and d), respectively, after subtraction of the Mg anode satellite lines; Sr *3d* and F *1s* peaks have been normalized to the same intensity, after additional removal of a Shirley-type background, for better comparison of the line shape and energy position; the experimental data are represented by dots, while solid lines are the fitting.

mobility and a progressive reduction of the sticking probability give rise to extended star-shaped 3D islands (Fig. 4c). Interestingly, at high-enough temperature, i.e. at 400 °C, the growth mode changes considerably. The sticking probability reduces further and the almost 'arrow-head' 3D structures do not develop, neither on top of terraces nor at step edges. Instead, the fluoride crystallites tend to merge and form long and narrow wires that stay locked to the step edges, leaving about 90 % of the surface substrate exposed. This may open interesting scenarios for application of 1D nanosized wires, or fibers, in nanophotonic and photonic integrated circuits. 1D dielectric wires can find relevant technological exploitation in light control as waveguides, in optical switches, in nanolasers, [34]. In many cases these 1D optical wires are obtained from organic materials [35–38]. The present study paves the way towards the self-assembly of purely inorganic 1D waveguides made of ionic fluorides, which represent one of the most relevant classes of optical materials. While organic wires may allow the transport of light as well as charges, in the present case electron conduction along the wire would be inhibited by the inorganic material, that would instead be suitable for light conduction and, eventually, exciton transmission. The possibility to dope the fluoride would further widen the application possibilities in active optical nanodevices. If doped with rare-earth ions (Eu^{3+} [39], Yb^{3+} [40] Er^{3+} [41]), fluoride nanowires would get unique luminescence properties that could find use as light emitters [42], scintillators [43] and biological labels [44]. Finally, cubic ionic fluorides are well known for their ionic transport capabilities, [45] which could now be tailored towards 1D nanoionic conduction. The observation and optimization of all these effects are outside of the objectives of the present work. As the development of methods for the synthesis of (fluoride) 1D nanostructure represents a key challenge in nanoscale industry [46,47], our study demonstrates that MBE can be used as a viable technique to fabricate these structures from bottom-up, through self-assembly, [48] thanks to a suitable choice of the substrate and exploiting the weak VdW attraction between HOPG and SrF_2.

5. Conclusions

A combination of experimental techniques has been used to investigate in detail the growth modes and the interaction of SrF_2 with HOPG, when SrF_2 is deposited by MBE. The atomic structure is accessed by RHEED and morphology of the films by AFM. Photoelectron spectroscopies with UV and X-ray photons are applied to get information on the valence band, work function, band offset, chemical reactivity of the fluoride at the interface with HOPG. The interaction between the fluoride and HOPG at the buried interface is very weak, of van der Walls nature. This guarantees a high mobility of the incoming molecules at all temperatures, from RT and above. 3D fluoride islands of dendritic form and bulklike composition nucleate at surface defects, mainly at the steps of the HOPG substrate, then propagating parallel and perpendicular to these. The crystal phase is that of the bulk material since the earliest stages of deposition. The film is not uniform, but it presents voids and cavities extending down to the substrate even at a nominal coverage of 5 nm, which is typically sufficient to completely cover the substrate when the growth is carried out over *3d* metals [12]. As the substrate temperature is increased during deposition, the 3D fluoride islands grow in their lateral size. Interestingly, this is accompanied by a sizable reduction of the molecular sticking coefficient. At 400 °C, the fluoride crystallites accumulate only in correspondence of the HOPG steps, guiding the self-assembly of very long and almost 1D dielectric wires. This opens

the intriguing possibility to apply MBE to grow 1D nanoscale optical guides and dielectric – nanoionic – wires.

CRediT authorship contribution statement

Mauro Borghi: Writing – review & editing, Writing – original draft, Validation, Methodology, Investigation, Formal analysis, Data curation, Conceptualization. **Giulia Giovanelli:** Methodology, Investigation, Formal analysis, Data curation. **Monica Montecchi:** Methodology, Investigation, Formal analysis, Data curation. **Raffaella Capelli:** Writing – review & editing, Methodology, Investigation. **Andrea Mescola:** Writing – review & editing, Investigation, Formal analysis, Data curation. **Guido Paolicelli:** Writing – review & editing, Methodology, Investigation, Formal analysis, Data curation. **Sergio D'Addato:** Writing – review & editing, Methodology, Formal analysis, Data curation. **Tibor Grasser:** Writing – review & editing, Validation, Supervision, Methodology, Funding acquisition, Conceptualization. **Luca Pasquali:** Writing – review & editing, Writing – original draft, Validation, Supervision, Project administration, Methodology, Investigation, Funding acquisition, Formal analysis, Data curation, Conceptualization.

Declaration of competing interest

The authors declare that they have no known competing financial interests or personal relationships that could have appeared to influence the work reported in this paper.

Data availability

Data will be made available on request.

Acknowledgements

We acknowledge financial support of the projects FAR2022MISSIONORIENTED-FOMO, title "FLUID"; FAR_DIP_2023_-DIEF, title 'Celis' and PRIN 2022 Project 'PETRA' (Project n. 2022T7ZSEK) in the frame of Next Generation EU. The European Research Council (ERC) under grant agreement no. 101055379 is also gratefully acknowledged. Dr Sergey Suturin is kindly acknowledged for helpful discussion and providing useful hints for electron diffraction interpretation.

Open Access Funding provided by Università degli Studi di Modena e Reggio Emilia within the CRUI-CARE Agreement.

References

[1] M. Schmidt, M.C. Lemme, H.D.B. Gottlob, F. Driussi, L. Selmi, H. Kurz, Mobility extraction in SOI MOSFETs with sub 1 nm body thickness, Solid State Electron. 53 (2009) 1246–1251, https://doi.org/10.1016/j.sse.2009.09.017.

[2] L.F. Register, E. Rosenbaum, K. Yang, Analytic model for direct tunneling current in polycrystalline silicon-gate metal-oxide-semiconductor devices, Appl. Phys. Lett. 74 (1999) 457–459, https://doi.org/10.1063/1.123060.

[3] A.A. Almutairi, Y. Zhao, D. Yin, Y. Yoon, Performance limit projection of germanane field-effect transistors, IEEE Electron Device Lett. 38 (2017) 673–676, https://doi.org/10.1109/LED.2017.2681579.

[4] D. Akinwande, C. Huyghebaert, C.H. Wang, M.I. Serna, S. Goossens, L.J. Li, H.S. P. Wong, F.H.L. Koppens, Graphene and two-dimensional materials for silicon technology, Nature 573 (2019) 507–518, https://doi.org/10.1038/s41586-019-1573-9.

[5] B. Radisavljevic, A. Radenovic, J. Brivio, V. Giacometti, A. Kis, Single-layer MoS_2 transistors, Nat. Nanotechnol. 6 (2011) 147–150, https://doi.org/10.1038/nnano.2010.279.

[6] W. Liao, W. Wei, Y. Tong, W.K. Chim, C. Zhu, Electrical performance and low frequency noise in hexagonal boron nitride encapsulated $MoSe_2$ dual-gated field effect transistors, Appl. Phys. Lett. 111 (2017) 082105, https://doi.org/10.1063/1.4993233.

[7] Y.Y. Illarionov, G. Rzepa, M. Waltl, T. Knobloch, A. Grill, M.M. Furchi, T. Mueller, T. Grasser, The role of charge trapping in MoS_2/SiO_2 and MoS_2/hBN field-effect transistors, 2D Materials 3 (2016) 035004. doi: 10.1088/2053-1583/3/3/035004.

[8] Y.Y. Illarionov, T. Knobloch, M. Jech, M. Lanza, D. Akinwande, M.I. Vexler, T. Mueller, M.C. Lemme, G. Fiori, F. Schwierz, T. Grasser, Insulators for 2D nanoelectronics: the gap to bridge, Nat. Commun. 11 (2020) 3385, https://doi.org/10.1038/s41467-020-16640-8.

[9] C. Wen, M. Lanza, Calcium fluoride as high-k dielectric for 2D electronics, Appl. Phys. Rev. 8 (2021) 021307, https://doi.org/10.1063/5.0036987.

[10] Y. Gao, H. Song, F. Zhou, W. Li, T. Li, Q. Wu, S. lin, T. Chen, T. Tong, Z. Fei, S. Yan, Y. Shi, Large-scale integration of CaF_2 with quasi-vdW interface on two-dimensional FETs, Appl. Phys. Lett. 124 (2024) 251602, https://doi.org/10.1063/5.0213065.

[11] L.J. Schowalter, R.W. Fathauer, R.P. Goehner, L.G. Turner, R.W. Deblois, S. Hashimoto, J.L. Peng, W.M. Gibson, J.P. Krusius, Epitaxial growth and characterization of CaF_2 on Si, J. Appl. Phys. 58 (1985) 302–308, https://doi.org/10.1063/1.335676.

[12] M. Borghi, A. Mescola, G. Paolicelli, M. Montecchi, S. D'Addato, S. Vacondio, L. Bursi, A. Ruini, B.P. Doyle, T. Grasser, L. Pasquali, Initial stages of growth and electronic properties of epitaxial SrF_2 thin films on Ag(111), Appl. Surf. Sci. 656 (2024) 159724, https://doi.org/10.1016/j.apsusc.2024.159724.

[13] Y. Sun, K. Schouteden, M. Recaman Payo, J.P. Locquet, J.W. Seo, Growth and characterization of ultrathin vanadium oxide films on HOPG, Nanomaterials 12 (2022) 1–12, https://doi.org/10.3390/nano12183134.

[14] A.S. Ahmed, H. Wen, T. Ohta, I.V. Pinchuk, T. Zhu, T. Beechem, R.K. Kawakami, Molecular beam epitaxy growth of SrO buffer layers on graphite and graphene for the integration of complex oxides, J. Cryst. Growth 447 (2016) 5–12, https://doi.org/10.1016/j.jcrysgro.2016.04.057.

[15] T.S. Cheng, A. Summerfield, C.J. Mellor, A. Davies, A.N. Khlobystov, L. Eaves, C. T. Foxon, P.H. Beton, S.V. Novikov, High-temperature molecular beam epitaxy of hexagonal boron nitride layers, J. Vac. Sci. Technol. BNanotechnology and Microelectronics: Materials, Processing, Measurement, and Phenomena 36 (2018) 02D103, https://doi.org/10.1116/1.5011280.

[16] G. Iannaccone, F. Bonaccorso, L. Colombo, G. Fiori, Quantum engineering of transistors based on 2D materials heterostructures, Nat. Nanotechnol. 13 (2018) 183–191, https://doi.org/10.1038/s41565-018-0082-6.

[17] A.K. Geim, I.V. Grigorieva, Van der Waals heterostructures, Nature 499 (2013) 419–425, https://doi.org/10.1038/nature12385.

[18] D. Nazzari, J. Genser, V. Ritter, O. Bethge, E. Bertagnolli, T. Grasser, W.M. Weber, A. Lugstein, Epitaxial growth of crystalline CaF_2 on silicene, ACS Appl. Mater. Interfaces 14 (2022) 32675–32682, https://doi.org/10.1021/acsami.2c06293.

[19] S. Wang, Y. Zhang, N. Abidi, L. Cabrales, Wettability and surface free energy of graphene films, Langmuir 25 (2009) 11078–11081, https://doi.org/10.1021/la901402f.

[20] A. Koma, Van der Waals epitaxy - a new epitaxial growth method for a highly lattice-mismatched system, Thin Solid Films 216 (1992) 72–76, https://doi.org/10.1016/0040-6090(92)90872-9.

[21] L. Pasquali, S.M. Suturin, A.K. Kaveev, V.P. Ulin, N.S. Sokolov, B.P. Doyle, S. Nannarone, Interface chemistry and epitaxial growth modes of SrF_2 on Si(001), Phys. Rev. B - Condensed Matter Mater. Phys. 75 (2007) 1–15, https://doi.org/10.1103/PhysRevB.75.075403.

[22] A. Ichimiya, P.I. Cohen, Reflection high-energy electron diffraction, Cambridge University Press, RHEED, 2004.

[23] A.E. Candia, L. Gómez, R.A. Vidal, J. Ferrón, M.C.G. Passeggi, An STM and Monte Carlo study of the AlF_3 thin film growth on Cu(111), J. Phys. D Appl. Phys. 48 (2015) 265305, https://doi.org/10.1088/0022-3727/48/26/265305.

[24] F. Calleja, J.J. Hinarejos, A.L. Vázquez De Parga, S.M. Suturin, N.S. Sokolov, R. Miranda, Epitaxial growth of CaF_2(111) on Cu(111) visualized by STM, Surf. Sci. 582 (2005) 14–20, https://doi.org/10.1016/j.susc.2005.03.003.

[25] D. Farías, K.F. Braun, S. Fölsch, G. Meyer, K.H. Rieder, Observation of a novel nucleation mechanism at step edges: LiF molecules on Ag(111), Surf. Sci. 470 (2000) L93–L98, https://doi.org/10.1016/S0039-6028(00)00917-1.

[26] A. Theodosiou, B.F. Spencer, J. Counsell, A.N. Jones, An XPS/UPS study of the surface/near-surface bonding in nuclear grade graphites: A comparison of monatomic and cluster depth-profiling techniques, Appl. Surf. Sci. 508 (2020) 144764, https://doi.org/10.1016/j.apsusc.2019.144764.

[27] H. Fukagawa, H. Yamane, T. Kataoka, S. Kera, M. Nakamura, K. Kudo, N. Ueno, Origin of the highest occupied band position in pentacene films from ultraviolet photoelectron spectroscopy: Hole stabilization versus band dispersion, Phys. Rev. B - Condensed Matter and Mater. Phys. 73 (2006) 24–26, https://doi.org/10.1103/PhysRevB.73.245310.

[28] R. Schlaf, B.A. Parkinson, P.A. Lee, K.W. Nebesny, N.R. Armstrong, Absence of final-state screening shifts in photoemission spectroscopy frontier orbital alignment measurements at organic/semiconductor interfaces, Surf Sci 420 (1999) L122–L129, https://doi.org/10.1016/S0039-6028(98)00850-4.

[29] J. Chen, Z. Zhang, Y. Guo, J. Robertson, Electronic properties of CaF_2 bulk and interfaces, J. Appl. Phys. 131 (2022) 215302, https://doi.org/10.1063/5.0087914.

[30] H. Ishii, K. Sugiyama, E. Ito, K. Seki, Energy level alignment and interfacial electronic structures at organic/metal and organic/organic interfaces, Adv. Mater. 11 (1999) 605–625, https://doi.org/10.1002/(SICI)1521-4095(199906)11:8<605::AID-ADMA605>3.0.CO;2-Q.

[31] M.R. Salehpour, S. Satpathy, G.P. Das, Electronic structure of the CaF2/Si(111) interface, Phys. Rev. B 44 (1991) 8880–8885, https://doi.org/10.1103/PhysRevB.44.8880.

[32] L. Pasquali, S.M. Suturin, V.P. Ulin, N.S. Sokolov, G. Selvaggi, A. Giglia, N. Mahne, M. Pedio, S. Nannarone, Calcium fluoride on Si(001): Adsorption mechanisms and epitaxial growth modes, Phys. Rev. B 72 (2005) 045448, https://doi.org/10.1103/PhysRevB.72.045448.

[33] M.A. Olmstead, R.I.G. Uhrberg, R.D. Bringans, R.Z. Bachrach, Photoemission study of bonding at the CaF_2-on-Si(111) interface, Phys. Rev. B 35 (1987) 7526–7532, https://doi.org/10.1103/PhysRevB.35.7526.

[34] Y.J. Li, X. Xiong, C.L. Zou, X.F. Ren, Y.S. Zhao, One-dimensional dielectric/metallic hybrid materials for photonic applications, Small 11 (2015) 3728–3743, https://doi.org/10.1002/smll.201500199.
[35] Y. Guo, L. Xu, H. Liu, Y. Li, C.M. Che, Y. Li, Self-assembly of functional molecules into 1D crystalline nanostructures, Adv. Mater. 27 (2015) 985–1013, https://doi.org/10.1002/adma.201403846.
[36] S. Chen, M.P. Zhuo, X.D. Wang, G.Q. Wei, L.S. Liao, Optical waveguides based on one-dimensional organic crystals, PhotoniX 2 (2021) 2, https://doi.org/10.1186/s43074-021-00024-2.
[37] L.C. Palmer, S.I. Stupp, Molecular self-assembly into one-dimensional nanostructures, Acc. Chem. Res. 41 (2008) 1674–1684, https://doi.org/10.1021/ar8000926.
[38] J. Xu, S. Semin, D. Niedzialek, P.H.J. Kouwer, E. Fron, E. Coutino, M. Savoini, Y. Li, J. Hofkens, H. Uji-I, D. Beljonne, T. Rasing, A.E. Rowan, Self-assembled organic microfibers for nonlinear optics, Adv. Mater. 25 (2013) 2084–2089, https://doi.org/10.1002/adma.201204237.
[39] X. Sun, Y. Li, Size-controllable luminescent single crystal CaF_2 nanocubes, Chem. Commun. 3 (2003) 1768–1769, https://doi.org/10.1039/b303614f.
[40] G. De, W. Qin, J. Zhang, D. Zhao, J. Zhang, Bright-green upconversion emission of hexagonal LaF_3: Yb 3+, Er3+ nanocrystals, Chem. Lett. 34 (2005) 914–915, https://doi.org/10.1246/cl.2005.914.
[41] H. Lian, J. Liu, Z. Ye, C. Shi, Synthesis and photoluminescence properties of erbium-doped BaF_2 nanoparticles, Chem. Phys. Lett. 386 (2004) 291–294, https://doi.org/10.1016/j.cplett.2004.01.036.
[42] L.F. Johnson, H.J. Guggenheim, Infrared-pumped visible laser, Appl. Phys. Lett. 47 (1971) 44–47, https://doi.org/10.1063/1.1653816.
[43] A.J. Wojtowicz, Rare-earth-activated wide bandgap materials for scintillators, Nucl. Instrum. Methods Phys. Res., Sect. A 486 (2002) 201–207, https://doi.org/10.1016/S0168-9002(02)00703-9.
[44] S. Sasidharan, A. Jayasree, S. Fazal, M. Koyakutty, S.V. Nair, D. Menon, Ambient temperature synthesis of citrate stabilized and biofunctionalized, fluorescent calcium fluoride nanocrystals for targeted labeling of cancer cells, Biomater. Sci. 1 (2013) 294–305, https://doi.org/10.1039/c2bm00127f.
[45] J. Maier, Nanoionics: Ion transport and electrochemical storage in confined systems, Materials for Sustainable Energy: A Collection of Peer-Reviewed Research and Review Articles from Nat. Publ. Group 4 (2010) 160–170, https://doi.org/10.1142/9789814317665_0023.
[46] M. Cao, C. Hu, E. Wang, The first fluoride one-dimensional nanostructures: microemulsion-mediated hydrothermal synthesis of BaF_2 whiskers, J. Am. Chem. Soc. 125 (2003) 11196–11197, https://doi.org/10.1021/ja036939c.
[47] B.Y. Mao, F. Zhang, S.S. Wong, Ambient template-directed synthesis of single-crystalline alkaline-earth metal fluoride nanowires, Adv. Mater. 18 (2006) 1895–1899, https://doi.org/10.1002/adma.200600358.
[48] D.K. Goswami, B. Satpati, P.V. Satyam, B.N. Dev, Growth of self-assembled nanostructures by molecular beam epitaxy, Curr. Sci. 84 (2003) 903–910. https://www.jstor.org/stable/24108052.